Detection of Small Portions of Water in VIS-NIR Images Acquired by UAVs

Daniel Trevisan Bravo, Stanley Jefferson de Araujo Lima,
Sidnei Alves de Araujo(✉), and Wonder Alexandre Luz Alves

Informatics and Knowledge Management Graduate Program,
Universidade Nove de Julho (UNINOVE), São Paulo, SP, Brazil
{danieltbravo,saraujo,wonder}@uni9.pro.br,
stanleyjefferson@outlook.com

Abstract. Water bodies detection in aerial images is a problem widely known and explored in the literature. However, the detection of small portions of water in satellite images is not usual due to their low spatial resolution. With the increasing use of Unmanned Aerial Vehicle (UAVs), this task becomes feasible from the point of view of spatial resolution, but suffers from the problem of low spectral resolution of the acquired images. In this sense, we have new challenges in dealing with an old problem. In this work we proposed an approach that combines Visible (VIS) and Near Infrared (NIR) aerial images, commonly acquired by sensors used in UAVs, for providing an indicative index for detecting small portions of water. This approach also includes a scheme to reconstitute visible spectral bands contaminated by the use of a special lens, coupled to visible RGB camera, to provide NIR spectral band. Experimental results evidenced the good accuracy of proposed approach in mapping small portions of water such as pools and fountains in VIS-NIR images, even in the cases where there is only a thin layer of water.

Keywords: Aerial images · Small portions of water · UAVs · Spectral bands · Genetic Algorithm

1 Introduction

The recognition of water features from remote sensing images has been widely explored in the last decades. It is usually solved using specific spectral bands, captured by sensors carried on satellites, which facilitates the creation of spectral signatures to characterize the patterns assigned to water bodies well as other elements such as soil and vegetation. Thus, several indices have been developed for detecting different features such as NDVI (Normalized Difference Vegetation Index), NDWI (Normalized Difference Water Index) and WII (Water Indicator Index).

In the last decade, we can find several proposals addressing the detection of large water bodies, such as oceans, rivers and lakes. Among them, we can cite Portz et al. [10], Qiao et al. [11], Zhao et al. [12] and Colet et al. [4].

The use of Unmanned Aerial Vehicle (UAVs), also known as drones, is an excellent alternative in remote sensing tasks, since they have the advantages of low cost, enabling flights closer to the ground and can produce high spatial resolution images. Thus, they have been widely used in recent years, especially in fields such as precision agriculture [2, 6], geosciences [5, 9] and health [1, 3, 7].

If on the one hand, the sensors carried by UAVs can acquire aerial images with high spatial resolution allowing the identification of small objects, on the other hand, they are very limited in terms of spectral resolution. Thus, new challenges have arisen such as the development of indices to characterize water, soil, vegetation and other elements, considering such limitations.

Murugan et al. [8] proposed an algorithm to select optimal subsets of spectral bands, aiming at the creation of indices indicative of water bodies and vegetation in satellite images. This algorithm makes an exhaustive search in 242 available spectral ranges, which may require a high computational cost. Nevertheless, the indices proposed for satellite-acquired images cannot be used in UAV-acquired images, since they have low spectral resolution and different ranges for the spectral bands.

Recently, Agarwal et al. [1] and Mehra et al. [7] addressed the identification of possible foci of the mosquito Aedes aegypti by means of image analysis, which were acquired by several types of devices, including UAVs' sensors. However, such works considers only the description of the scenes by means of a bag of features extracted from the images, without considering the detection of water features.

In fact, there are many approaches to detect large water bodies in satellite images. However, no work addressing the recognition of small portions of water in images acquired by UAVs was found in our literature review. One of the reasons may be the high cost of multispectral cameras with specific sensors, that can be used for detecting water. In this context, we explore in this paper how to detect small portions of water in aerial images acquired by a low-cost UAV equipped with a visible RGB camera adapted with a lens to capture the NIR spectral band. The procedures proposed in this work could, for example, make more robust the approach developed by Murugan et al. [8], which constitutes an important practical application for detecting foci of the mosquito Aedes aegypti.

2   Materials and Methods

For conducting the experiments, we acquired a dataset of 50 images from an area of the campus of São Paulo University – USP (central coordinate with latitude/longitude -23.5614311 and -46.7198984), located in the city of São Paulo/Brazil. We employed a DJI Phantom 3 professional UAV carrying on board a Sony EXMOR camera of 12.4 MP, capable of acquiring images of 4000×3000 pixels. Using a special lens (focal length 3.97 mm; aperture 2.8; 16 MP; 82°) this camera can provide the NIR spectral band. The flight was carried out 50 m above the ground, with a planned spatial resolution of 2.2 cm, on September 5, 2016 at 11:00 am, with a duration of approximately 20 min. We chose an area of the campus containing small portions of water discovered such as pools and fountains.

Each pixel of the acquired images is described as follows: $I\_NIR(x, y) = \{NIR(x, y), \tilde{G}(x, y), \tilde{R}(x, y)\}$, where NIR, $\tilde{G}$ and $\tilde{R}$ are the Near Infrared, green and red bands, respectively. It is important to highlight that the lens coupled in the RGB camera to obtain NIR has larger bandwidths and captures the data at different wavelengths causing nonlinear reflectance contamination in the bands G and R. Thus, we denote these contaminated bands as $\tilde{G}$ and $\tilde{R}$.

Since this contamination causes imprecision in the computation of indices indicative of water that depend on these bands, we proposed a procedure to reconstitute them using a Multilayer Perceptron Artificial Neural Network (MLP-ANN). In other words, we employed this procedure to generate an RGB image from I_NIR. To train the MLP-ANN, we also acquired 5 images from the same area of the USP using the RGB camera without the NIR lens, maintaining the same UAV flying parameters. An image of this second dataset is represented as: $I\_VIS(x, y) = \{R(x, y), G(x, y), B(x, y)\}$, where R, G and B are the visible bands red, green and blue. Such images were correlated with NIR images, using an image registration operation, to compose 5 pairs VIS-NIR from which we extracted the training set.

Finally, a Genetic Algorithm (GA) was designed to produce an optimized indicative index of water (OIIW), which is useful to filter pixels representing small portion of water in the images.

The experiments described in this work were performed using MATLAB R2015 running on an Intel i7 processor of 2.5 GHz speed and 8 GB RAM.

3   Proposed Approach

The proposed approach includes 3 parts: reconstitution of visible spectral bands, creation of the optimized indicative index of water (OIIW) and detection of small portions of water, which are described in Sects. 3.1 to 3.3.
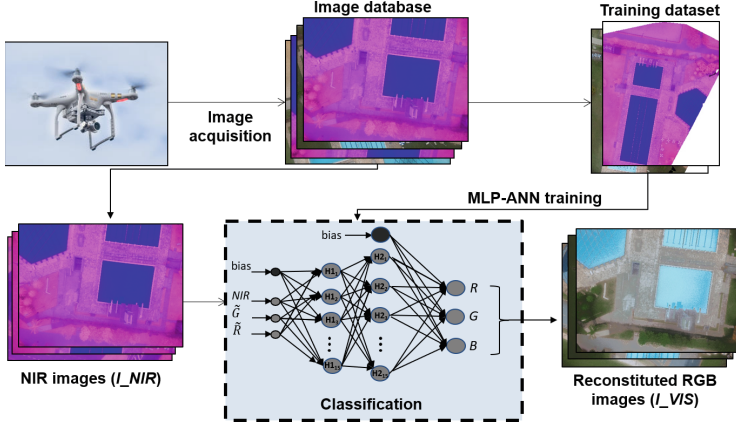
3.1   Reconstitution of Visible Spectral Bands

Due to the contamination in the bands $\tilde{G}$ and $\tilde{R}$, already explained in the previous section, a MLP-ANN was employed to reconstitute I_VIS from I_NIR, as illustrated in Fig. 1.

To compose the dataset for training the MLP-ANN, we extracted manually 60 sub images with 50×50 pixels from the 5 pairs (used only for training) of correlated VIS-NIR images. In summary, for each pixel chosen in an RGB image, it was extracted a sub image from that image and from its correspondent NIR at the same position. Thus, each instance of training is described by the following 6 attributes: $NIR, \tilde{G}, \tilde{R}, R, G, B$, being the first three extracted from I_NIR (inputs) and the last three from I_VIS sub images (expected outputs).

Formally, the function of developed MLP-ANN is to map each set $\{NIR(x, y), \tilde{G}(x, y), \tilde{R}(x, y)\}$ into another set $\{R(x, y), G(x, y), B(x, y)\}$. Then, all mapped sets make up the pixels of the reconstituted RGB image. This procedure is important because it avoids the conduction of two complete

missions to acquire the RGB and NIR images from the same area, impacting directly on the time spent in the image acquisition task as well as saving the battery of the UAV. In addition, the proposed OIIW depends on VIS and NIR spectral bands.

Fig. 1. Working of proposed approach for reconstitution of visible spectral bands.

3.2   Creation of the Optimized Indicative Index of Water (OIIW)

A Genetic Algorithm (GA) was designed to provide the OIIW, as illustrated in Fig. 2. Each chromosome of GA encodes a set of 4 values (c_1, b_1, c_2 and b_2) that compose the index, as follows: $OIIW = \frac{c_1 b_1 - c_2 b_2}{c_1 b_1 + c_2 b_2}$, where $b_i \in [1, 4]$ indicate the selected bands from the set NIR, R, G, B and $c_i \in [0.1, 10.0]$ are the weights applied to these bands. Obviously, b_i are integer values while c_i are real values.

The objective function (f) to evaluate the solutions of GA (Eq. 1) consists in minimizing the total similarity S between pairs of images (in our case, 3 pairs), each one consisting of an image provided by using of OIIW encoded in a GA solution (I_OIIW) and another binary image annotated manually to indicate the expected result (I_EXP). Examples of these images are shown in Fig. 3.

$$Minimize \quad f(c_1, b_1, c_2, b_2) = \sum_{j=1}^{3} S(I\_OIIW_j, I\_EXP_j) \tag{1}$$

In the experiments, we adopted the Mean Absolute Error (MAE), described in Eq. 2, to measure the similarity (S) between a pair of images:

$$S(I\_OIIW, I\_EXP) = \frac{1}{MN} \sum_{m=0}^{M-1} \sum_{n=0}^{N-1} |I\_OIIW_{m,n} - I\_EXP_{m,n}| \tag{2}$$

where M and N are the dimensions of the images being compared. It is important to emphasize that any other measure of similarity could be employed in Eq. 2.
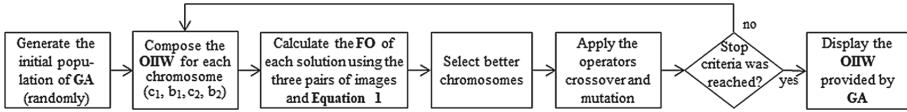
Fig. 2. Steps of designed GA to provide the OIIW.

Some GA configuration parameters were: population size $= 250$; number of generations $= 400$ (used as stop criteria); population rate of replacement $= 0.8$; crossover $= 0.85$; mutation rate $= 0.10$. After the convergence of GA, we obtained the OIIW given by Eq. 3.

$$OIIW = \frac{6.855NIR - 2.3475B}{6.855NIR + 2.3475B} \tag{3}$$

The bands suggested by GA to compose the OIIW are in consonance with the literature, since many researches in remote sensing area indicate a combination of the NIR and VIS bands for detecting bodies of water. This is due to the fact that water presents high absorption in the NIR range and the bands of the visible spectrum, when combined with NIR, allow to characterize water quality. Finally, the importance of determination the weights for each band, made by GA, must be highlighted. Such weights are responsible for the fine adjustment in the indices and, as may be observed in the literature, they are usually obtained empirically or exhaustively.

In Fig. 3 it can be observed that the images generated using proposed OIIW (column d) were very similar to the annotated images (column c), evidencing the good results obtained. In both columns, the regions of images containing water are indicated by gray levels near to black.
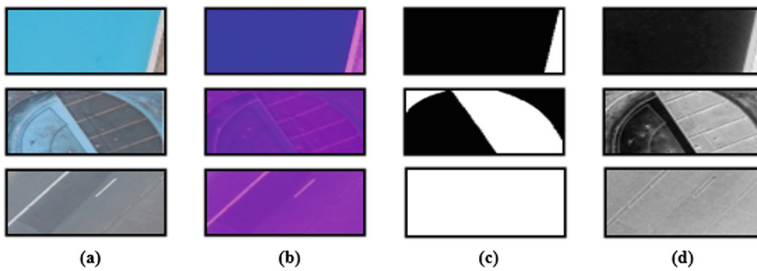
Fig. 3. Some results obtained with the created OIIW. (a) RGB images (I_VIS); (b) NIR images (I_NIR); (c) Images with the expected results (annotated images); (d) Images generated by OIIW considering the bands NIR and B extracted from images shown in columns a and b.

3.3   Detection of Small Portions of Water

The detection of small portions of water from a pair VIS-NIR images is performed by calculating the Eq. 3 (OIIW), which considers NIR and B spectral bands. This procedure generates a greyscale image I_GRAY in which the pixels are real values ranging from 0.0 to 1.0, being the portions of water represented by gray levels near to zero (black).

The final step consists in converting I_GRAY in a binary image I_BIN through a simple binarization algorithm using a threshold of 0.85 (obtained empirically). Thus, the pixels of I_BIN with value 0 indicate water.

4   Experimental Results

In this section, we present qualitative and quantitative results obtained in the experiments conducted. First, we apply the MLP-ANN in the 50 NIR images of the main dataset, to reconstitute their corresponding RGB versions aiming at the decontamination of spectral bands $\tilde{G}$ and $\tilde{R}$. Two reconstituted images are shown in the column c of Fig. 4. When comparing these images with the original RGB images, showed in the column b, it can be observed that the results are very satisfactory. Also based on a qualitative analysis, it is possible to observe from the images depicted in the columns d and e that the proposed approach for detection small portions of water presented good results.
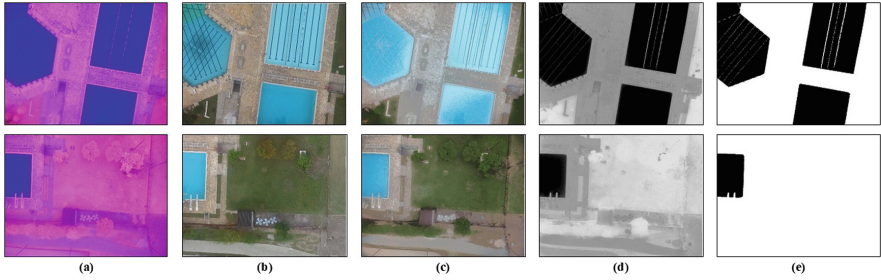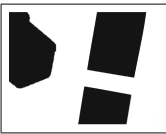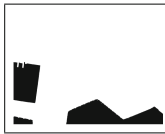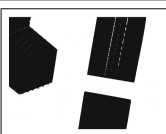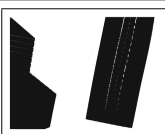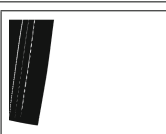
Fig. 4. Results of detection of small portions of water. (a) NIR images (I_NIR); (b) Original RGB images (I_VIS); (c) Reconstituted RGB images; (d) Images resulting from the application of the OIIW (I_GRAY); (e) Binary images (I_BIN).
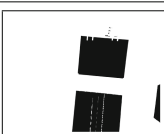
In the Table 1 we present some quantitative results obtained with the application of OIIW on a subset of 10 images (this subset includes all images containing bodies of water), for which we manually create the annotated versions with regions containing water highlighted in black. The quality of results is indicated by the measures Mean Absolute Error (MAE) and Structural Similarity Index ($SSIM$), which are widely used to express the similarity between images. It is possible to observe that the results were satisfactory, since the values obtained by MAE very close to 0. In addition, the average value of $SSIM$ (0.9768) also

indicates that the resulting images are very similar to their annotated versions, considering that the maximum similarity between two images occurs when the value of $SSIM$ is equal to 1.

Finally, it is important to highlight that although the proposed procedure for providing OIIW considers only 4 spectral bands, it could be easily adapted for a larger number of bands adjusting the GA chromosome. In addition, our approach is much more efficient, in terms of computational cost, than that proposed by Murugan et al. [8].

Table 1. Quantitative results obtained from experiments considering annotated images (first and forth lines: annotated images; second and fifth lines: images generated by applying OIIW; third and sixth lines: MAE and SSIM values, respectively)

| 0.0100 ; 0.9732 | 0.0068 ; 0.9736 | 0.0003 ; 0.9978 | 0.0350 ; 0.9345 | 0.0030 ; 0.9904 |

| 0.0072 ; 0.9830 | 0.0067 ; 0.9811 | 0.0036 ; 0.9879 | 0.0013 ; 0.9946 | 0.0016 ; 0.9949 |

5   Conclusion

In this work, we proposed an approach to detect small portions of water in aerial images acquired by UAVs. It includes an optimized indicative index of water (OIIW) and a procedure do decontaminate visible spectral bands in images acquired by a RGB camera using a special lens to provide NIR band. Regarding the detection of water, the obtained results show that, in general, the proposed approach presents a good precision in detecting pools and fountains even in the

cases where there is only a thin layer of water. Thus, this approach could be employed, for example, to map possible foci of Aedes aegypti mosquitoes. With respect to the experiments involving the reconstitution of visible spectral bands, it can be verified that the resulting images were well reconstituted, being very useful to compute OIIW. In future works we intend to carry out new experiments replacing the techniques of Neural Networks and Genetic Algorithms by a Deep Convolutional Neural Network.

References

1. Agarwal, A., Chaudhuri, U., Chaudhuri, S., Seetharaman, G.: Detection of potential mosquito breeding sites based on community sourced geotagged images. In: SPIE 9089, Geospatial InfoFusion and Video Analytics IV and Motion Imagery for ISR and Situational Awareness II (2014). https://doi.org/10.1117/12.2058121
2. Candido, A.K.A.A., Silva, N.M., Filho, A.C.P.: High resolution images of unmanned aerial vehicles (UAV) in the planning of land use and occupation. Anuario do Instituto de Geociencias - UFRJ **38**, 147–156 (2015)
3. Capolupo, A., Pindozzi, S., Okello, C., Boccia, L.: Indirect field technology for detecting areas object of illegal spills harmful to human health: applications of drones, photogrammetry and hydrological models. Geospatial Health **8**(3), 699–707 (2014). https://doi.org/10.4081/gh.2014.298
4. Colet, M.E., Braun, A., Manssour, I.H.: A new approach to turbid water surface identification for autonomous navigation. In: 24th International Conference in Central Europe on Computer Graphics, Visualization and Computer Vision (WSCG 2016), pp. 317–326 (2016)
5. Gaitani, N., Burud, I., Thiis, T., Santamouris, M.: High-resolution spectral mapping of urban thermal properties with unmanned aerial vehicles. Build. Environ. **121**, 215–224 (2017)
6. Long, D., McCarthy, C.L., Jensen, T.: Row and water front detection from UAV thermal-infrared imagery for furrow irrigation monitoring. In: 2016 IEEE International Conference on Advanced Intelligent Mechatronics (AIM), pp. 300–305 (2016)
7. Mehra, M., Bagri, A., Jiang, X., Ortiz, J.: Image analysis for identifying mosquito breeding grounds. In: 2016 IEEE International Conference on Communication and Networking (SECON Workshops), pp. 1–6 (2016). https://doi.org/10.1109/SECONW.2016.7746808
8. Murugan, P., Sivakumar, R., Pandiyan, R., Annadurai, M.: Algorithm to select optimal spectral bands for hyperspectral index of feature extraction. Indian J. Sci. Technol. **9**(37), 1–13 (2016)
9. Oliveira, L.S.B., Bezerra, F.H.R.: Karstification fault identification in the potiguar using UAV/drone images. In: XVII Brazilian Symposium on Remote Sensing, pp. 6148–6152 (2015)
10. Portz, L., Guasselli, L.A., Correa, I.C.S.: Spatial and temporal variation of NDVI in lagoa do peixe. Revista Brasileira de Geografia Fisica **4**(5), 897–908 (2011)

11. Qiao, C., Luo, J., Sheng, Y., Shen, Z., Zhu, Z., Ming, D.: An adaptive water extraction method from remote sensing image based on NDWI. Indian Soc. Remote Sens. **40**(3), 421–433 (2012)
12. Zhao, Y., Deng, Y., Pan, C., Guo, L.: Research of water hazard detection based on color and texture features. Sens. Transducers **157**(10), 428–433 (2013)